

# Thermodynamics of Water in an Enzyme Active Site: Grid-Based Hydration Analysis of Coagulation Factor Xa

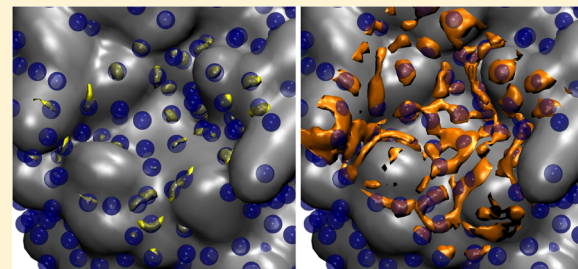
Crystal N. Nguyen,<sup>†</sup> Anthony Cruz,<sup>‡</sup> Michael K. Gilson,<sup>\*,†</sup> and Tom Kurtzman<sup>\*,‡</sup>

<sup>†</sup>Skaggs School of Pharmacy and Pharmaceutical Sciences, University of California San Diego, 9500 Gilman Drive, La Jolla, California 92093-0736, United States

<sup>‡</sup>Department of Chemistry, Lehman College, The City University of New York, 250 Bedford Park Blvd. West, Bronx, New York 10468, United States

## Supporting Information

**ABSTRACT:** Water molecules in the active site of an enzyme occupy a complex, heterogeneous environment, and the thermodynamic properties of active-site water are functions of position. As a consequence, it is thought that an enzyme inhibitor can gain affinity by extending into a region occupied by unfavorable water or lose affinity by displacing water from a region where it was relatively stable. Recent advances in the characterization of binding-site water, based on the analysis of molecular simulations with explicit water molecules, have focused largely on simplified representations of water as occupying well-defined hydration sites. Our grid-based treatment of hydration, GIST, offers a more complete picture of the complex distributions of water properties, but it has not yet been applied to proteins. This first application of GIST to protein–ligand modeling, for the case of Coagulation Factor Xa, shows that ligand scoring functions based on GIST perform at least as well as scoring functions based on a hydration-site approach (HSA), when applied to exactly the same simulation data. Interestingly, the displacement of energetically unfavorable water emerges as the dominant factor in the fitted scoring functions, for both GIST and HSA methods, while water entropy plays a secondary role, at least in the present context.



## 1. INTRODUCTION

The binding of a drug-like molecule to a protein leads to displacement of water molecules from the protein's binding pocket, and the thermodynamics of this displacement process is thought to contribute significantly to the overall thermodynamics of protein–ligand binding.<sup>1–14</sup> For example, displacement of water that is tightly bound via multiple water–protein hydrogen bonds may incur a large energetic penalty, whereas displacement of water from hydrophobic parts of the binding pocket may help drive ligand-binding. Intuitively, one may view different parts of the protein's surface as imposing different surface energies on the nearby water, with correspondingly different thermodynamic consequences for water displacement by various ligands.

The use of molecular distribution functions<sup>15–21</sup> to analyze molecular dynamics (MD) simulations has led to important advances in the study of binding site water and its role in molecular recognition; parallel progress with the 3D RISM approach<sup>22–24</sup> also deserves mention but is not considered here. Key early contributions include development of Water-Map<sup>8,12</sup> (Schrödinger LLC), STOW,<sup>25</sup> and other approaches,<sup>26,27</sup> which have provided new insight and shown promise as tools to help discover small molecules that will bind a targeted binding pocket. Such methods frequently define spherical sites, where water is present at high density, to represent the distribution of water in the binding site. This

hydration site approach (HSA) is motivated in part by the practical consideration that, in regions where water is present at lower density, it becomes more difficult to obtain converged values of the local orientational entropy of water. This is a simple consequence of the lower number of water samples available from the simulation in such low-density locations. The HSA strategy of limiting attention to hydration sites where water is present at high density maximizes the chances for good numerical convergence of the orientational entropy. However, as previously discussed,<sup>28</sup> the regions in a binding site where water is present at high density can have a complex shape, which is not easily represented by a collection of spheres.

This limitation has been addressed in a grid-based implementation of inhomogeneous solvation theory (IST), termed GIST.<sup>28,29</sup> Instead of constructing hydration sites, GIST discretizes the smooth distributions of water density and other properties onto a fine, three-dimensional grid. The problem of converging the local orientational entropy of water is overcome through the use of a highly efficient nearest-neighbor (NN) method, as opposed to histogram methods, which require more

**Special Issue:** Free Energy Calculations: Three Decades of Adventure in Chemistry and Biophysics

**Received:** December 27, 2013

**Published:** April 3, 2014

sampling to reach adequate convergence.<sup>30,31</sup> GIST can also take advantage of the fact that regions of lower density contribute proportionately less than regions of higher density regions to the overall orientational entropy of the displaced water. This density-weighting means that, if one is interested in the integral of the orientational entropy over a volume containing both high and low density regions, one can converge the overall integral to an acceptable tolerance, so long as the high-density regions are well converged. Alternatively, the grid approach makes it straightforward to focus on regions where water is present at high density, as done in HSA, without simplifying their shapes.

Here, we describe the first test of GIST for a ligand–protein system. In order to establish a clear basis for comparing methods, we study coagulation factor Xa (FXa) with a set of small molecule inhibitors used in early studies of the WaterMap method,<sup>12</sup> and we derive scoring functions based on both GIST and HSA methods. For this initial test of GIST’s applicability to protein–ligand modeling, we do not seek to establish a full-fledged protein–ligand scoring function, suitable for virtual screening or lead optimization. Instead, as previously done,<sup>12</sup> we ask how well the GIST treatment of hydration can capture affinity differences between closely related congeneric pairs of ligands, where differences in binding affinity that result from contributions other than solvation such as configurational entropy and protein–ligand energy are minimal. Our results support the applicability of GIST and, in addition, provide an unexpected outcome regarding the role of energetically versus entropically unfavorable water.

## 2. METHODS

We ran explicit-water MD simulations of FXa and used both GIST and our local HSA implementation to extract information about the structure and thermodynamics of the water in the binding site. We then considered the displacement of this binding site water by various FXa inhibitors, whose binding site poses are known or could be inferred from the known poses of very similar compounds. Candidate scoring functions, based on the computed properties of the water displaced by each ligand, were trained on subsets of the experimental affinity data and then tested on separate sets, in order to assess the utility of the hydration data to resolve the relative binding affinities of pairs of congeneric ligands. Details of the computational methods are presented in the following subsections.

### 2.1. Grid Inhomogeneous Solvation Theory (GIST).

**2.1.1. GIST Implementation.** As previously detailed, GIST uses a three-dimensional rectangular grid of cubic voxels in the region of interest and processes the snapshots of an MD trajectory to compute the following thermodynamic quantities for each voxel,  $k$ , centered at location  $\mathbf{r}_k$ :

- $\Delta E_{k,sw}^{\text{norm}}$ , the mean solute–water interaction energy of a water molecule in voxel  $k$ .
- $\Delta E_{k,ww}^{\text{norm}}$ , one-half the mean interaction energy of the water in voxel  $k$  with all other waters. The factor of  $1/2$ , which was not included in the definition of the corresponding water–water interaction energy in our initial presentation of GIST,<sup>28</sup> is customary in liquid-state theory; it allows the total energy of neat water to be written as the sum of the individual water energies.
- $-T\Delta S_{k,sw}^{\text{trans,norm}}$ , the single-body (one-water) translational entropy of water in voxel  $k$ , relative to bulk, normalized to the mean number of waters in the voxel.

- $-T\Delta S_{k,sw}^{\text{orient,norm}}$ , the single-body (one-water) orientational entropy of water in voxel  $k$ , relative to bulk, normalized to the mean number of waters in the voxel.

Note that we previously used a somewhat different notation for these quantities;<sup>29</sup> for example,  $\Delta E_{k,sw}^{\text{norm}}$  was  $\Delta E_{sw}^{\text{norm}}(\mathbf{r}_k)$ . Here, a  $20.5 \times 20.5 \times 22.5 \text{ \AA}$  grid was centered on the active site of FXa. The grid spacing of  $0.5 \text{ \AA}$  provides voxels large enough to give statistically meaningful data but small enough to still give a high resolution description of the density distribution functions.<sup>28</sup> It is worth noting that the volume of each voxel is 33.5 times less than that of a hydration site (see below), as the latter represents a sphere of radius  $1 \text{ \AA}$ . The GIST Lennard-Jones and electrostatic energies were computed from stored MD frames, using the minimum image convention and no cutoff, and the reference value of the bulk water–water interaction energy was computed in the same convention. The main GIST calculations presented here used 100 000 frames saved at 1 ps intervals during a 100 ns production MD run, but shorter durations were also examined, to study convergence, as detailed below.

**2.1.2. Functional Form of GIST-Based Scoring Functions.** When a ligand binds a protein, it displaces water from the protein’s binding site. If the displaced water was unfavorable relative to bulk, then water displacement should make a favorable contribution to the ligand’s binding affinity. With this in mind, we initially looked for a correlation between measured ligand binding affinities and regional hydration free energies (eq 25 of ref 28), where the region was defined as those voxels covered by each ligand in a bound pose. However, finding little correlation (data not shown), we conjectured that any underlying correlation had been obscured by noise, due to sharp variations in the hydration energies with even small changes in ligand position. This sharpness traces, at least in part, to our use of a single pose for each ligand, and a restrained protein structure in the water simulations. We addressed this issue by constructing scoring functions which are based on the GIST data but are less sensitive to the details of local water properties, due to the use of cutoffs in local water density, energy, and entropy. The use of cutoffs to construct a well-behaved scoring function from local hydration data was first introduced in the context of a hydration site model.<sup>12</sup>

We tested three such scoring functions based on the GIST hydration data available from the grid described above. In all three cases, voxel  $k$  can contribute to a ligand’s score only if the voxel’s center,  $\mathbf{r}_k$ , lies within the van der Waals radius of any atom of the ligand. For a given ligand, then, each voxel is assigned a binary displacement indicator,  $d_k$ , which equals 1 if the center of the voxel lies within the van der Waals radius of any ligand atom and 0 if it does not. The van der Waals radii are drawn from the software package Crystal Maker (Crystal-Maker Software Ltd.), which in turn relies on Bondi.<sup>32</sup> We also allowed the scoring function to focus on voxels where water is present at high density by setting up an additional binary indicator,  $g_k$ , which is set to 1 if the water density in voxel  $k$  exceeds a cutoff  $g_{co}$ , and 0 if it does not. This cutoff is one of the trained parameters, so it will be greater than zero only if imposing a density cutoff actually improves the accuracy of the scoring function. Finally, we set up similar cutoffs for the total energy and entropy,  $E_k^{\text{norm}}$  and  $-T\Delta S_{k,sw}^{\text{norm}}$ , associated with each voxel  $k$ , and used these to define additional binary masks based on energy and entropy thresholds. Thus, the binary mask,  $e_k$ , equals 1 if  $E_k^{\text{norm}}$  exceeds the cutoff,  $E_{co}$ , and 0 otherwise; and the binary mask,  $s_k$ , equals 1 if  $-T\Delta S_{k,sw}^{\text{norm}}$  exceeds the cutoff,  $S_{co}$ ,

and 0 otherwise. Like the density cutoff,  $g_{\text{co}}$ , the values of  $E_{\text{co}}$  and  $S_{\text{co}}$  are fitted parameters and hence are free to go to zero if imposing these cutoffs does not improve the accuracy of the scoring function. The total energy and entropy were computed as  $E_k^{\text{norm}} \equiv \Delta E_{k,\text{sw}}^{\text{norm}} + 2\Delta E_{k,\text{ww}}^{\text{norm}} - 2E_{\text{ww,bulk}}^{\text{norm}}$  and  $-T\Delta S_{k,\text{sw}}^{\text{norm}} \equiv -T\Delta S_{\text{trans,norm}}^{\text{norm}} - T\Delta S_{\text{orient,norm}}^{\text{norm}}$ , respectively. The quantity  $E_k^{\text{norm}}$  is the mean interaction energy of the water in voxel  $k$  with the protein and all other waters, relative to what its interactions would be in bulk,  $2E_{\text{ww,bulk}}^{\text{norm}}$  computed in the same convention as the other GIST quantities.

With the voxels' binary masks in place for density, energy, and entropy, we now define the three candidate scoring functions, one using both the energy and entropy data from GIST, the second using only the energy data, and the third using only the entropy data:

$$\begin{aligned}\Delta G_{\text{ES}} &= E_{\text{aff}} \sum_k d_{kg_k} e_k + S_{\text{aff}} \sum_k d_{kg_k} s_k + C \\ \Delta G_E &= E_{\text{aff}} \sum_k d_{kg_k} e_k + C \\ \Delta G_S &= S_{\text{aff}} \sum_k d_{kg_k} s_k + C\end{aligned}\quad (1)$$

Here,  $E_{\text{aff}}$  and  $S_{\text{aff}}$  are additional fitted parameters, which specify the affinity increments provided by voxels surpassing the energy and entropy cutoffs, respectively, and also meeting the criteria  $d_k = g_k = 1$ . Note that in this study, each of these scoring functions was trained separately and has its own fitted values of  $g_{\text{co}}$  and  $C$ , as well as  $E_{\text{co}}$  and  $E_{\text{aff}}$  and/or  $S_{\text{co}}$  and  $S_{\text{aff}}$ .

**2.1.3. Training and Testing of the GIST-Based Scoring Function.** We adjusted the scoring functions described above to fit the measured relative binding free energies,  $\Delta\Delta G_{\text{expt}}$ , of 28 different congeneric pairs of FXa inhibitors (see below). Separate training and test sets were used, in order to avoid overfitting of the parameters. Thus, we used a random number generator to split the 28 pairs into two arbitrarily selected sets of 14 apiece. Ten such random splits were carried out, creating 10 distinct training and test sets. Parameters were optimized for each training set and then tested on the corresponding test set. We report means and standard deviations over these 10 splits for the resulting fitted parameters and accuracy metrics. We further assess the significance of these results by comparing them with results obtained after a shuffling operation, which used the `gsl_permutation` function in the GNU Scientific Library, to randomly exchange the entropy and enthalpy values among pairs of voxels.

For each training set, the parameters were adjusted as follows, using  $\Delta G_{\text{ES}}$  as an example. We scanned values of  $E_{\text{co}}$  and  $S_{\text{co}}$  from 0 to 4 kcal/mol and values of  $g_{\text{co}}$  from 0 to 4 (in units of neat water density), each in increments of 0.1. This scan yields  $41 \times 41 \times 41 = 68\,921$  combinations of the three cutoff values. For each combination, the sums in eq 1 were computed for all ligands. Linear regression was then used to obtain values of  $E_{\text{aff}}$  and  $S_{\text{aff}}$  that provide the highest correlation coefficient ( $R^2$ ) of the relative scores for the congeneric pairs,  $\Delta\Delta G_{\text{ES}}$ , to the corresponding experimental values,  $\Delta\Delta G_{\text{expt}}$ , for the training set. The optimized values of the five fitted parameters were then used to compute  $\Delta\Delta G_{\text{ES}}$  for the congeneric pairs in the training set, and the reliability of the scoring function was evaluated based on the resulting value of  $R^2$  for the test set. Analogous procedures were used for the other two scoring functions,  $\Delta G_E$  and  $\Delta G_S$ . These require

scanning only  $41 \times 41 = 1681$  cutoff combinations and yield only one of the two affinity parameters,  $E_{\text{aff}}$  or  $S_{\text{aff}}$ , rather than both as for  $\Delta G_{\text{ES}}$ .

**2.2. Hydration Site Analysis (HSA).** **2.2.1. Assignment of Thermodynamic Properties to Hydration Sites.** Hydration sites in the FXa binding site were defined and analyzed thermodynamically based on the same MD simulation used for the GIST calculations, using the first 10 ns (10 000 frames), in accord with the common practice of using approximately 2–10 ns simulations for HSA calculations.<sup>12,27,33–35</sup> We used every 10th frame of this segment to identify the hydration sites. We first collected all instances, in these 1000 frames, of water molecules within 5 Å of any heavy atom of any bound ligand (see below). For each water molecule in this set, we counted the number of neighboring waters from the same set, using the criterion of an oxygen–oxygen distance within 1 Å. With this definition, a water molecule can count as its own neighbor, if two instances of it in different frames meet the distance criterion. The location of the first hydration site was then set to the coordinates of the water oxygen with the most neighbors. This water molecule and all of its neighbors were then removed from consideration as potential hydration sites, and the location of the next hydration site was set to the coordinates of the remaining water oxygen with the most neighbors, based on the initial counts. This removal process was iterated until the number of neighbors of all remaining waters was less than twice that expected for a 1000 frame simulation of bulk water (i.e., < 280 from 1000 frames). Each hydration site then was associated with all water instances, from the full 10 000 MD frames (above), whose oxygens lay within 1 Å of the site.

Each hydration site  $i$  was associated with a mean energy  $E_i$  and a one-body entropy  $S_i$ . The energy of a water molecule in a given hydration site was calculated as half the difference between the total energy of the water–protein system with the water present and without it. A script invoking the program AMBER,<sup>36</sup> with settings matched to those of the MD simulation, was used to compute these energies. The mean energy of the hydration site then is the average of these energies for all water molecules that populate the site, minus the average energy of a water molecule in neat water from matched calculations. The water entropy  $S_i$  associated with hydration site  $i$  is the sum of its one-body translational and orientational entropies,  $S_{i,\text{sw}}^{\text{trans}} \equiv -k\rho \int_{V_{hs}} g(\mathbf{r}) \ln g(\mathbf{r}) \, d\mathbf{r}$  and  $S_{i,\text{sw}}^{\text{orient}} \equiv ((-kN_i)/\Omega) \int_{V_{hs}} g(\omega) \ln g(\omega) \, d\omega$ , where  $\mathbf{r}$  is position in the

protein frame of reference,  $k$  is Boltzmann's constant,  $\rho$  is bulk water density,  $g(\mathbf{r})$  is the local water density referenced to bulk,  $N_i$  is the number of water molecules associated with hydration site  $i$ ,  $\Omega \equiv 8\pi^2$ ,  $V_{hs}$  indicates an integral restricted to the spherical hydration site, and  $\omega$  defines orientational coordinates in the protein frame of reference. The translational entropy was computed by the histogram method, where spherical coordinates  $r, \theta, \phi$  centered on the hydration site were divided into uniformly spaced bins in  $r, \cos \theta, \phi$  to generate 512 three-dimensional bins of equal volume, with  $r \in [0, 1]$  Å,  $\theta \in [0, \pi]$ , and  $\phi \in [0, 2\pi]$ . The orientational entropy associated with a hydration site was computed via the same nearest neighbor method used by GIST for individual voxels.<sup>28</sup>

**2.2.2. HSA-Based Scoring Function.** We used the hydration sites described above as the basis for three cutoff-based scoring functions, whose functional forms build on prior work.<sup>12</sup> Like

the three GIST scoring functions (above), the free HSA-based scoring functions are based on, respectively, both energy and entropy, energy alone, and entropy alone:

$$\begin{aligned}\Delta G_{\text{ES}} &= E_{\text{aff}} \sum_i d_i e_i + S_{\text{aff}} \sum_i d_i s_i + C \\ \Delta G_E &= E_{\text{aff}} \sum_i d_i e_i + C \\ \Delta G_S &= S_{\text{aff}} \sum_i d_i s_i + C\end{aligned}\quad (2)$$

Here, the sums range over hydration sites  $i$ ;  $e_i$  and  $s_i$  equal 1 if  $E_i$  and  $-TS_i$  are greater than cutoff values  $E_{\text{co}}$  and  $S_{\text{co}}$ , respectively, and 0 otherwise;  $d_i$  is a displacement function, defined below, which accounts for the overlap of the ligand, in a given pose, with hydration site  $i$ ;  $E_{\text{aff}}$  and  $S_{\text{aff}}$  are fitted constants; and  $C$  is a constant offset. Note that the HSA scoring parameters in eq 2 are set independently of the GIST scoring parameters in eq 1, despite the use of some equivalent symbols.

We tried two forms of the displacement function. One is identical to that used in the previous paper,<sup>12</sup> while the second, as discussed below, applies a physically motivated cap to this quantity:

$$\begin{aligned}d_i^{\text{nocap}} &= \sum_j^{\text{atoms}} \Theta(R_{\text{co}} - R_{ij}) \left( \frac{R_{\text{co}} - R_{ij}}{R_{\text{co}}} \right) \\ d_i^{\text{cap}} &= \min[1, d_i^{\text{nocap}}]\end{aligned}\quad (3)$$

Here,  $\Theta(x)$ , the Heaviside step function, equals 0 if  $x \leq 0$  and 1 otherwise;  $R_{\text{co}}$  is a distance cutoff;  $R_{ij}$  is the distance between hydration site  $i$  and atom  $j$  of the ligand being scored; and the sum runs over all atoms belonging to the ligand being scored,  $i$ . For  $d_i^{\text{nocap}}$ , which is modeled on the prior hydration site scoring function,<sup>12</sup> each ligand atom within  $R_{\text{co}}$  of the hydration site makes a contribution that scales between 0 and 1 as it approaches the center of the site, so the displacement function accounts for the degree to which a ligand displaces the water in the site. However, this approach is nonphysical in the sense that, if  $R_{ij} < R_{\text{co}}$  for multiple ligand atoms  $j$  and a single site  $i$ , then the displacement of solvent from the site may be multiply counted. That is, for the energy/entropy scoring function, a site might contribute more than  $E_{\text{aff}} + S_{\text{aff}}$ ; for the energy-only scoring function, it might contribute more than  $E_{\text{aff}}$ ; and for the entropy-only scoring function, it might contribute more than  $S_{\text{aff}}$ . Indeed, in the present study, we found values of  $d_i^{\text{nocap}}$  up to 3.2, implying that a single site might contribute over three times. We therefore also considered the alternative displacement function,  $d_i^{\text{cap}}$ , which is capped at a value of 1, so that no hydration site may contribute more than one-fold to a ligand's score, in accordance with the fact that the site cannot be displaced more than once.

**2.2.3. Training and Testing of the HSA-Based Scoring Function.** The parameters of the HSA-based scoring functions were adjusted in the same manner as those of the GIST-based scoring functions, except that  $R_{\text{co}}$  took the place of  $g_{\text{co}}$ . Thus, values of  $R_{\text{co}}$  were scanned from 2 to 3 Å, in steps of 0.1 Å and, as for GIST, values of  $E_{\text{co}}$  and  $S_{\text{co}}$  were scanned from 0 to 4 kcal/mol in increments of 0.1 kcal/mol. (Note that no hydration sites had energies greater than 3.7 kcal/mol.) The sums in eq 2 were evaluated for each ligand and with each combination of  $R_{\text{co}}$ ,  $E_{\text{co}}$ , and  $S_{\text{co}}$ . For each set of cutoffs scanned, values of  $E_{\text{aff}}$  and  $S_{\text{aff}}$  were obtained by linear regression against

the differences in measured binding free energies for a training set of congeneric ligand pairs, for each scoring function in eq 2. The parameters that yielded the highest correlation coefficients were chosen and were tested for their ability to reproduce the difference in binding affinities for the congeneric pairs in the test set. This procedure was applied to the same 10 training and test sets used for the GIST scoring function. As done for GIST, we assessed the significance of the HSA results by comparing them with results obtained after a shuffling operation, which randomly exchanges the entropy and enthalpy values across pairs of hydration sites.

**2.3. Molecular Systems and Modeling.** **2.3.1. Molecular Dynamics Simulations of Binding Site Water.** Both GIST and the HSA methods take as input a Boltzmann sample of water configurations for a given configuration of the protein. Here, we used molecular dynamics (MD) simulations to generate this sample from the canonical ensemble (NVT), as follows. We used the structure of FXa from Protein Data Bank<sup>37,38</sup> entry 1FJS,<sup>39</sup> as previously done,<sup>12</sup> and our assignment of protonation states was also consistent with this prior study. We removed the ligand from the binding site and used Tleap and other Amber Tools<sup>36</sup> to assign protein parameters from the AMBER99sb force field<sup>40</sup> and solvate the protein with 8557 TIP3P water molecules.<sup>41</sup> The simulations used a periodic box with dimensions 66.5 Å × 72.2 Å × 60.9 Å, which afforded at least 10 Å between any protein atom and the edge of the periodic box. Four disulfide bonds were set up to join cysteine pairs 7/12, 27/43, 156/170, and 181/209, and two ions observed in the crystal structure ( $\text{Ca}^{2+}$  and  $\text{Cl}^-$ ) were restrained to their original positions. The resulting simulation system had 29 338 atoms, comprising the protein, the two ions, and the water molecules.

Energy minimization, followed by MD simulation, was carried out with the Amber 12 software using pmemd.cuda<sup>42</sup> on a single GPU. First, the energy of the system was minimized in two rounds; both used 1500 steps of the steepest descents algorithm followed by the conjugate gradient method for a maximum of 2000 steps. In the first round, all protein atoms were harmonically restrained to their initial positions with a force constant of 100 kcal/mol/Å<sup>2</sup>. In the second round, the system was further relaxed keeping only non-hydrogen protein atoms restrained, with the same force constant. The energy minimized system was then heated with a series of 20 ps constant-volume and -temperature MD simulations with the first simulation at 50 K and the temperature incremented by 50 K every 20 ps until 300 K was reached. The system was then equilibrated for 10 ns at 300 K at a constant pressure of 1 atm. At the final volume, the system was then equilibrated for an additional 5 ns at constant volume. The final MD production run of 100 ns was at constant number of particles, volume, and temperature (NVT), and system configurations were stored every 1 ps, for a total of 100 000 stored configurations. During all MD simulations, all protein atoms were harmonically restrained to their positions following the energy minimization step, with a force constant of 100 kcal/mol/Å. The SHAKE algorithm<sup>43</sup> was used to constrain the lengths of all bonds involving hydrogen atoms. Temperature was regulated by Langevin dynamics with a collision frequency of 2.0 ps<sup>-1</sup>. A 9 Å cutoff was applied to all nonbonded interactions. Particle mesh Ewald was implemented to account for long-range electrostatic interactions, and the Leapfrog algorithm was used to propagate the trajectory. For the constant pressure simulations, isotropic position scaling was implemented with a pressure relaxation

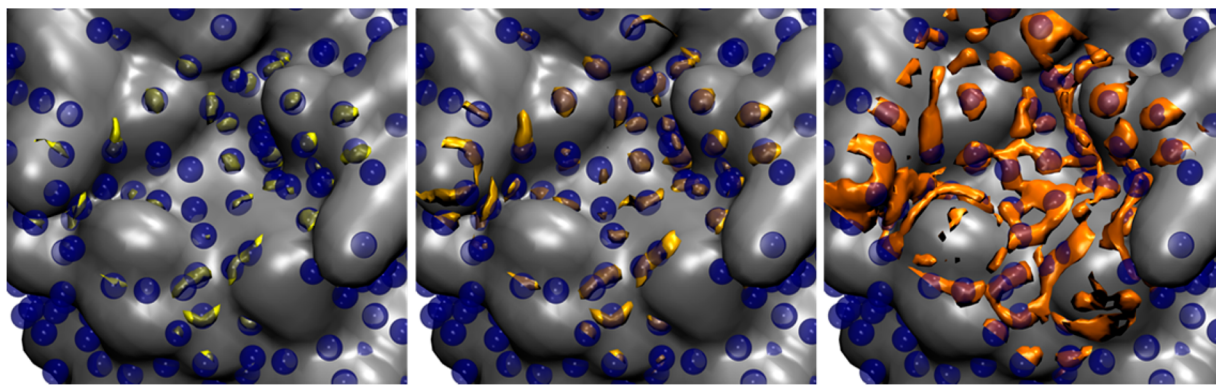


**Figure 1.** Comparison of the GIST and HSA representations of water density in the Factor Xa binding pocket. HSA sites (blue spheres) are the same in all three panels. From left to right, the GIST contour levels are at  $g = 6, 4$ , and  $2$ . The GIST water densities are based on the occupancy of grid voxels by water oxygens, and the boundaries of the grid box may be discerned in the right-hand panel. A smoothed protein surface is shown in order to highlight the water data.

time of  $0.5$  ps. The main GIST and HSA solvation maps were produced from these configurations. However, in order to study the convergence properties of GIST, we performed two additional  $20$  ns NVT production runs storing configurations every  $0.05$  ps; one was begun identically with the  $100$  ns run, and the other was begun with the last MD configuration of the  $100$  ns run.

**2.3.2. Ligand Data Set and Preparation.** We trained and tested the scoring functions with a set of  $28$  congeneric ligand pairs (see Supporting Information), where the members of each pair differ only by small, localized chemical changes in rigid moieties, leading to differential displacement of solvent. As previously discussed,<sup>12</sup> this approach minimizes the contributions of free energy terms other than hydration and thus allows a focus on the quantity of central interest in this study. The  $28$  pairs used here are a subset of  $31$  drawn from several experimental series<sup>44–55</sup> for use in a previous computational study;<sup>12</sup> we eliminated three pairs (Matter:25/Matter:28; Matter:28/2BMG:I1H; Mueller:3/Mueller:2), because we were not confident of the conformation of at least one member of the pair, and hence of the location of the displaced solvent. In particular, Mueller:3 differs from Mueller:2 by a phenyl group whose orientation is not clear, because it is attached by a rotatable bond; and for the other two pairs, an aromatic ring changes to a nonaromatic ring, whose conformation is uncertain. It is worth noting that, for this set of ligands, there is essentially no correlation between binding free energy and molecular weight ( $R^2 = 0.12$ ).

Ligand poses were drawn from available cocrystal structures or generated from a cocrystal structure of a closely related ligand by a small chemical adjustment. In all cases, the cocrystal structure was aligned with the simulated protein (above) to generate an initial pose in the binding site for which the hydration structure was computed. Final poses for modeling solvent displacement were generated by protonating the ligands, then minimizing the initial poses in the simulated protein structure while allowing the ligand and protein hydrogen atoms to relax. The atomic partial charges for each ligand were obtained from the restrained electrostatic potential (RESP) method,<sup>56</sup> using quantum-mechanically derived electrostatic potentials with the 6-31G\* basis set. Other ligand force field parameters were obtained using GAFF.<sup>57</sup> Note that these parameters were used only to generate the ligand poses studied with the GIST and HSA scoring functions.

### 3. RESULTS

#### 3.1. Comparison of Grid and Site Representations of Water Density.

The HSA hydration sites are informative about water density but do not capture the level of detail available from GIST's grid-based method. The two approaches are compared in Figure 1, which displays the HSA sites (blue spheres) computed for the binding pocket of Factor Xa, along with GIST's gridded representation of water density, contoured at three different levels. Contours of water density at  $6$  times that of bulk ( $g = 6$ ) appear as discrete, mostly convex droplets (yellow contours, left panel), although a few of these high-density regions are elongated, rather than round. Every high-density droplet is matched by a spherical HSA site, but there are many HSA sites in the binding pocket that do not enclose one of these high-density droplets. Contours at  $4$  times bulk density ( $g = 4$ ) appear as more and larger droplets and match the HSA sites rather well (gold contours, middle panel). Contours at twice bulk density ( $g = 2$ ) form long, curved strands, which follow the contours of the protein surface (orange contours, right panel), and are not well represented by the HSA sites. These begin to delineate the first hydration shell of the protein. Finally, contours at still lower density (e.g.,  $g = 1.5$ ) include parts of the second hydration shell (not shown). Overall, the HSA representation captures the droplet-like distribution of the highest water densities but does not distinguish between high and medium density regions and does not capture the complex distributions of water density that become apparent at densities roughly twice that of bulk. This observation has practical relevance, because the scoring functions developed here include regions where water density is of this order, as detailed in the next subsection.

It is also worth remarking that a hydration site should not be directly equated with a single bound water, as the sites' occupancies are typically well below one. Thus, for the HSA sites within  $5$  Å of the bound ligands, we find a mean occupancy of  $0.58$  waters molecules, with a standard deviation of  $0.22$ . These values are similar to those reported previously for Factor Xa in an early implementation of WaterMap:<sup>12</sup> the occupancies reported in Table 1 of the prior report correspond to a mean of  $0.51$  water molecules per hydration site, with a standard deviation of  $0.22$ .

**3.2. GIST scoring functions.** A GIST-based scoring function based on both the local energy and one-body entropy of displaced water yields good correlations with the measured

Table 1. Scoring Functions Based on GIST and HSA Water Calculations<sup>a</sup>

			test $R^2$	train $R^2$	$g_{co}$ or $R_{co}$	$E_{co}$	$S_{co}$	$E_{aff}$	$S_{aff}$	C
actual	GIST	E/S	0.84 ± 0.06	0.94 ± 0.02	1.90 ± 0.32	0.62 ± 0.42	3.34 ± 0.46	-0.18 ± 0.05	0.08 ± 0.05	-0.23 ± 0.20
		E	0.85 ± 0.05	0.92 ± 0.02	1.62 ± 0.57	0.65 ± 0.42	N.A.	-0.14 ± 0.04	N.A.	-0.23 ± 0.19
		S	0.35 ± 0.11	0.49 ± 0.11	2.52 ± 0.69	N.A.	2.13 ± 0.44	N.A.	-0.10 ± 0.08	-0.50 ± 0.31
HSA Nocap	HSA Nocap	E/S	0.80 ± 0.07	0.88 ± 0.05	2.81 ± 0.28	0.28 ± 0.08	1.87 ± 0.50	-1.70 ± 0.31	0.09 ± 0.60	-0.36 ± 0.26
		E	0.83 ± 0.07	0.85 ± 0.06	2.91 ± 0.07	0.30 ± 0.06	N.A.	-1.50 ± 0.15	N.A.	-0.43 ± 0.14
		S	0.67 ± 0.10	0.66 ± 0.11	2.57 ± 0.17	N.A.	2.25 ± 0.05	N.A.	-1.52 ± 0.33	-0.68 ± 0.33
HSA Cap	HSA Cap	E/S	0.66 ± 0.24	0.86 ± 0.07	2.35 ± 0.19	0.48 ± 0.52	2.10 ± 0.62	-2.44 ± 2.51	-0.18 ± 1.75	-0.47 ± 0.23
		E	0.80 ± 0.08	0.83 ± 0.06	2.38 ± 0.06	0.28 ± 0.08	N.A.	-2.31 ± 0.31	N.A.	-0.53 ± 0.19
		S	0.69 ± 0.12	0.72 ± 0.08	2.53 ± 0.09	N.A.	2.09 ± 0.26	N.A.	-2.38 ± 0.38	-0.50 ± 0.26
shuffled	GIST	E/S	0.42 ± 0.20	0.85 ± 0.06	2.45 ± 0.80	1.74 ± 1.14	1.19 ± 1.01	-0.52 ± 1.94	-0.44 ± 1.12	-0.64 ± 0.61
		E	0.35 ± 0.20	0.62 ± 0.15	2.50 ± 0.75	0.36 ± 0.93	N.A.	0.24 ± 2.17	N.A.	-0.72 ± 0.70
		S	0.44 ± 0.16	0.69 ± 0.11	1.91 ± 1.24	N.A.	1.56 ± 1.17	N.A.	-0.89 ± 0.65	-0.59 ± 0.45
HSA Nocap	HSA Nocap	E/S	0.44 ± 0.18	0.82 ± 0.08	2.89 ± 0.13	-1.52 ± 1.62	1.84 ± 1.39	0.12 ± 1.84	-0.88 ± 1.75	-0.57 ± 0.30
		E	0.46 ± 0.14	0.50 ± 0.16	2.81 ± 0.06	-3.30 ± 2.20	N.A.	-0.90 ± 0.34	N.A.	-0.79 ± 0.32
		S	0.38 ± 0.18	0.57 ± 0.19	2.85 ± 0.10	N.A.	2.02 ± 1.17	N.A.	-1.26 ± 0.90	-0.75 ± 0.31
HSA Cap	HSA Cap	E/S	0.36 ± 0.20	0.78 ± 0.13	2.85 ± 0.09	-1.54 ± 2.26	1.96 ± 1.49	-0.34 ± 4.79	-3.32 ± 4.05	-0.67 ± 0.30
		E	0.17 ± 0.16	0.36 ± 0.17	2.86 ± 0.12	-2.48 ± 1.78	N.A.	-1.48 ± 1.30	N.A.	-0.95 ± 0.37
		S	0.28 ± 0.24	0.47 ± 0.22	2.89 ± 0.13	N.A.	2.00 ± 0.99	N.A.	-2.06 ± 1.36	-0.90 ± 0.28

<sup>a</sup>The quality of each scoring function is reported in terms of coefficients of determination ( $R^2$ ). The test-set results (test  $R^2$ ) are the most meaningful; the training-set results (train  $R^2$ ) are included for completeness. All quantities are averages across the 10 splits, with associated standard deviations. Results are presented for the actual hydration data and for hydration data shuffled among voxels (GIST) or hydration sites (HSA), and HSA results are presented for capped and uncapped displacement functions (see Methods). Scoring functions were constructed based on both energy and entropy data (E/S), energy data only (E), and entropy data only (S); the parameters are defined in the Methods section.

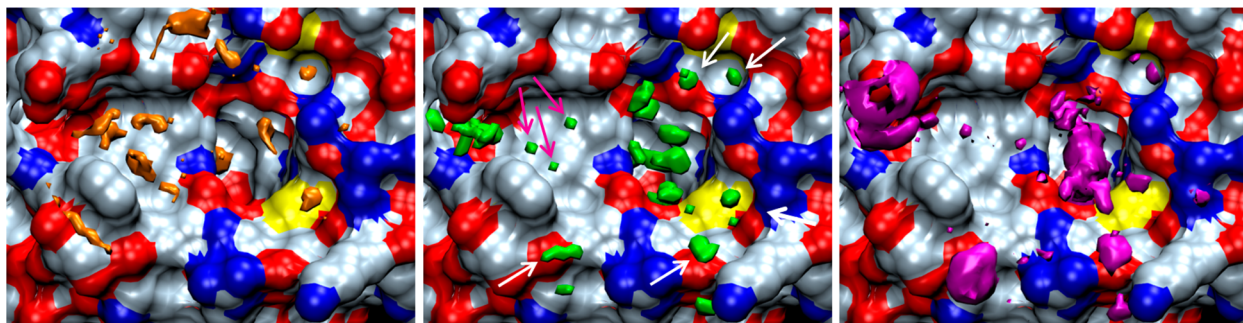
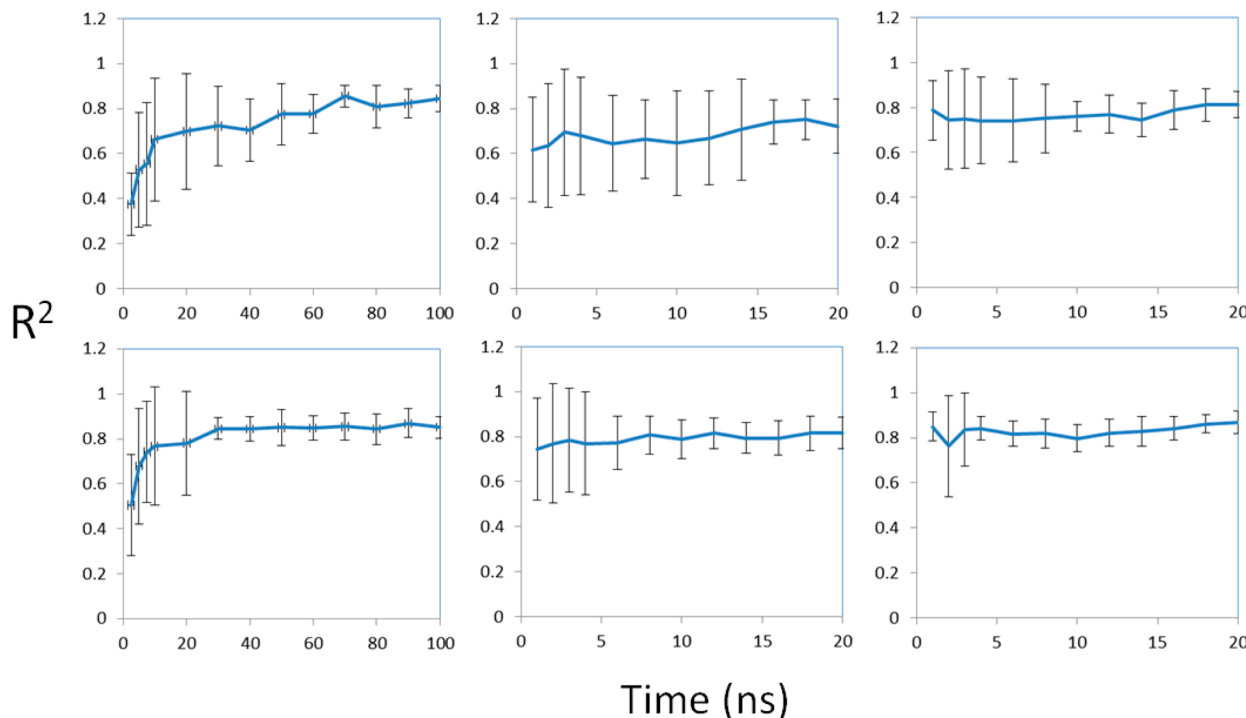


Figure 2. GIST contours in binding site of FXa, in molecular surface representation. Left: Energy scoring region, which meets both density and energy cutoff criteria for the combined energy–entropy scoring function. Middle: Entropy scoring region, which meets both density and entropy cutoff criteria for the combined energy–entropy scoring function. Right: Normalized total water energy, contoured at -2.6 kcal/mol/water. White arrows: entropy scoring subregions at the polar surface. Magenta arrows: entropy scoring subregions at hydrophobic surface. Red: oxygen. Blue: nitrogen. Pale blue: carbon. Graphic generated with VMD.<sup>58</sup>

binding affinity differences for the 28 congeneric ligand pairs (Table 1, top row). The mean  $R^2$  value is 0.94 across 10 training sets drawn at random from the full set of 28 pairs, and a high correlation ( $R^2 = 0.84$ ) is preserved when the optimized parameters are applied to the respective test sets. The best results are obtained when voxels are excluded if their water density is less than about twice the bulk density ( $g_{co} = 1.9$ ). Each voxel which furthermore meets the energy cutoff (about 0.6 kcal/mol/water above bulk) contributes about -0.2 kcal/mol of affinity. The entropy terms are somewhat puzzling: the entropy cutoff of 3.3 kcal/mol/water is much higher than the energy cutoff of 0.6 kcal/mol/water, and the positive value of  $S_{aff}$  seemingly indicates that displacing low entropy water disfavors binding, rather than favoring it, as might be

anticipated. These results suggest that the energy term may be more meaningful; this topic is further discussed below.

It is of interest to visualize the energy and entropy scoring regions; i.e., those voxels which meet either both the density and energy cutoffs or both the density and entropy cutoffs, respectively. As shown in Figure 2 (left), the energy scoring region tends to localize at extended regions of the nonpolar surface. These are places where water molecules lose more energy due to desolvation by the protein than they gain by making new interactions with the protein. (The projection from three to two dimensions makes some scoring regions appear deceptively close to polar protein atoms.) The analogous visualization for the energy-only scoring function, which is discussed below, is very similar (data not shown). The locations of the entropy scoring regions (Figure 2, middle) are more



**Figure 3.** Convergence of  $R^2$  values for GIST scoring functions, as a function of simulation duration. Top row: combined energy/entropy scoring function. Bottom row: energy-only scoring function. Left: 100 ns simulation, frames saved at 1 ps intervals. Middle: The first 20 ns of the same 100 ns simulation, frames saved every 0.05 ps. Right: 20 ns simulation initiated from the last frame of the 100 ns simulation, frames saved every 0.05 ps.

complicated. Some (white arrows) lie at the surface of polar atoms; others (pink arrows) lie at hydrophobic locations. The frequent localization of entropy scoring regions at polar surfaces, and the unexpectedly positive value of  $S_{\text{aff}}$ , likely reflects the fact that polar surfaces can tightly bind waters, leading to unfavorable entropies but favorable energies (Figure 2, right) typical of traditional entropy–enthalpy compensation. Displacement of water from such regions may be net unfavorable, and this might help account for the positive value of  $S_{\text{aff}}$ . On the other hand, the displacement of entropically disfavored water from subregions where energy is not particularly favorable should favor ligand binding. Thus, the energetically mixed nature of the entropic scoring regions further suggests that it may not give a clear signal in the overall scoring function.

In order to study the significance of the energy and entropy terms in more detail, we also considered a scoring function based only on density and energy, and another based only on density and entropy. As shown in Table 1 (second and third rows), the energy-only scoring function performs just as well ( $R^2 = 0.85$  for the test sets) as the original one based on both energy and entropy. In addition, the fitted parameters are similar in magnitude and sign to those of the original energy term. In contrast, the entropy-only scoring function yielded a poor correlation with experimental data ( $R^2 = 0.35$  for the test sets), and the sign of  $S_{\text{aff}}$  is reversed relative to that in the original scoring function. Thus, the hydration energy alone carries all of the predictive power of the GIST-based scoring function, at least for FXa with this ansatz. This result is consistent with the analysis of the combined energy/entropy scoring function, above.

As a further check of the statistical significance of the present results, we shuffled the GIST data among voxels and then refitted all three GIST-based scoring functions using the

shuffled data. The results are presented in the lower half of Table 1. This procedure was repeated with three independent randomizations. Although correlations as high as  $R^2 = 0.82$  are obtained for the training sets, the test-set results are all poor ( $R^2 \approx 0.4 \pm 0.2$ ). This result supports the significance of the high correlations obtained with the true (unshuffled) data and indicates that the low correlations observed for the entropy-only scoring function should be viewed as statistically insignificant.

Finally, we examined the amount of MD simulation data required to generate the high correlations observed above. First, we reanalyzed the original set of MD frames, which had been saved at 1 ps intervals. For increasing numbers of frames from this set, we reran the 10 training and test calculations and computed the mean and standard deviation of the resulting 10 values of  $R^2$ . As shown in Figure 3 (left), the value of  $R^2$  and its standard deviation (error bars) appear to plateau at about 60 ns for the combined energy–entropy scoring function (top left). Interestingly, the plateau starts much earlier, at about 30 ns, for the energy-alone scoring function (lower left). It appears that the more slowly convergent entropy term delays convergence of the energy–entropy scoring function, so that leaving out the entropy term in the energy-only scoring function speeds convergence. This result is, again, consistent with the irrelevance of the entropy term in the GIST scoring functions. We then asked whether shorter MD simulations might give better convergence if frames were saved at shorter time intervals. First, we reprocessed the first 20 ns of the same simulation, now processing frames saved at 0.05 ps. As shown in Figure 3 (top middle), the combined energy/entropy scoring function now converges somewhat more quickly, especially as measured by the reduction in the standard deviation of  $R^2$  across the 10 train/test calculations. The improvement is more marked for the energy-only scoring function, as well-converged

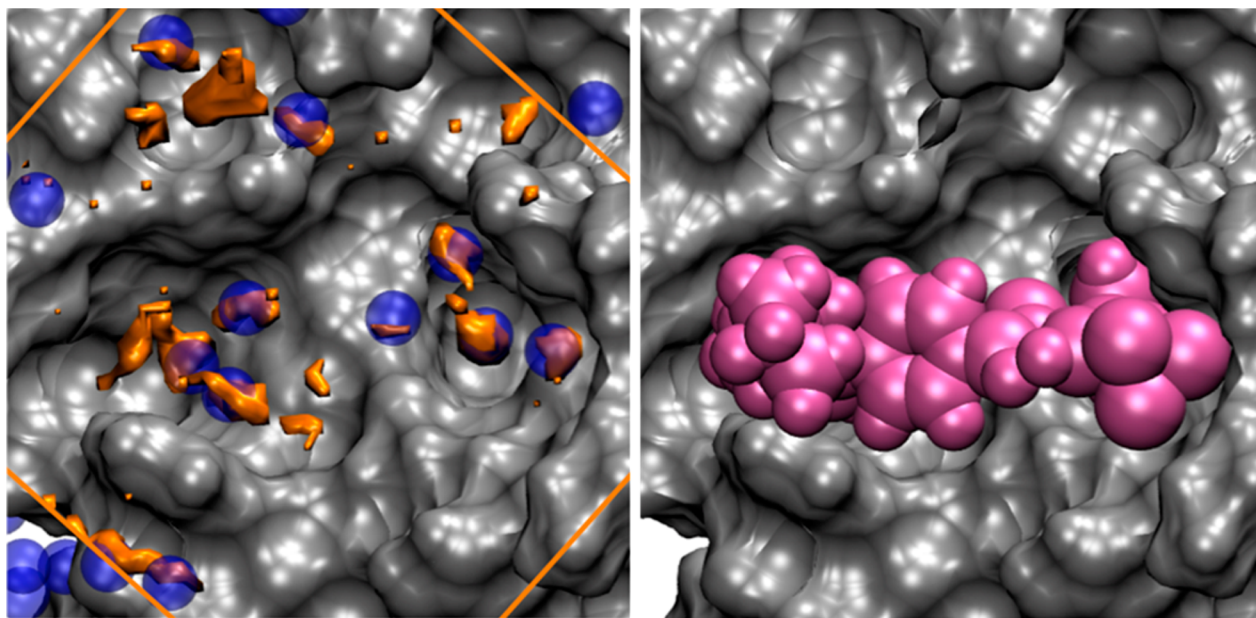


**Figure 4.** Comparison of GIST and HSA scoring locations, in the context of the FXa binding site (gray). Left: Scoring sites from the capped HSA energy-only scoring function (blue spheres) and energy scoring regions from the GIST energy-only scoring function (orange contours). GIST results are present only within the limits of the GIST grid (orange lines). Right: a representative ligand, PDB HET ID 4QC, in van der Waals representation (pink).

results are now available after only 10 ns of simulation time, although the standard deviation of  $R^2$  remains slightly higher than that from the 100 ns simulation. We then extended the 100 ns simulation by 20 ns, saving frames at 0.05 ps intervals, and examined convergence over this short simulation. The results are further improved, with good convergence and tight error bars achieved within about 5 ns for the energy-only scoring function, and 10 ns for the combined energy/entropy one. The improvement in these results, relative to those from the early 20 ns segment, suggests that the water structure continued to equilibrate somewhat during the 100 ns run, so it would have been appropriate to use a somewhat longer equilibration period in the MD protocol. In summary, at least for FXa, a simulation of 10 ns or less suffices to gain all the benefit of these GIST scoring functions.

**3.3. HSA-Based Scoring Functions.** As discussed in the Methods section, a prior HSA scoring function was constructed in such a way that the thermodynamic contribution of each hydration could be counted multiple times, if more than one ligand atom lay within a cutoff distance.<sup>12</sup> This function gave good results but is arguably nonphysical, because once the water in a hydration site has been displaced, it cannot be displaced again. Here, we present results for a set of similarly constructed HSA-based scoring functions in which, as before, a hydration site can be counted multiple times; as well as a second set, in which the contribution of each hydration site is capped, so that it can only contribute once. For both the uncapped and capped models, we examine scoring functions based on energy and entropy, energy only, and entropy only, as also done for GIST.

With the original uncapped approach, where a hydration site can contribute multiple times, the combined energy/entropy scoring function provides high correlation coefficients for both the training ( $R^2 = 0.88$ ) and test ( $R^2 = 0.80$ ) sets (Table 1, fourth row, marked E/S). These values of  $R^2$  are slightly lower than those for GIST, but the difference is not statistically

significant. Interestingly, the fitted value of  $E_{\text{aff}}$  (-1.70 kcal/mol) is much greater than that of  $S_{\text{aff}}$ , which in fact is assigned a positive sign (0.09 kcal/mol). In addition, the training procedure puts much sharper constraints on the energy terms than the entropy terms, as indicated by the fact that the standard deviations of  $E_o$  and  $E_{\text{aff}}$  (0.08 and 0.31 kcal/mol, respectively) are lower than those for  $S_o$  and  $S_{\text{aff}}$  (0.50 and 0.60 kcal/mol). Thus, the training results suggest that the entropy term is of lower importance than the energy term, much as observed in the case of GIST. Accordingly, a scoring function based entirely on energy (Table 1, row 5, marked E) performs as well as the one with both energy and entropy, and furthermore yields values of  $R_{\text{co}}$ ,  $E_{\text{co}}$ , and  $E_{\text{aff}}$  very similar to those of the combined energy–entropy scoring function. On the other hand, an entropy-only scoring function (Table 1, row 6, marked S) also performs fairly well, with a value of  $R^2 = 0.66$  for the test sets, and the fitted value of  $S_{\text{aff}} = -1.52$  kcal/mol, is essentially the same as the fitted value of  $E_{\text{aff}}$  for the energy-only scoring function, -1.50 kcal/mol. Thus, the entropy-only scoring function appears to largely replicate the energy-only scoring function, with some drop in the correlation with experimental data. These results are similar to those for GIST, as in both cases, the energy-only scoring function performed as well as the energy/entropy one, while the entropy-only one is worse. However, the decline in performance on going to entropy-only is much greater for GIST than for HSA.

In the second variant of the HSA-based scoring functions, no hydration site can contribute more than one-fold to the difference between two ligands' affinities. Imposing this physically reasonable cap on the contribution of each site reduced the experimental correlation of the scoring function with experimental data to 0.66 for the test sets with the combined energy–entropy scoring function but had essentially no effect on the correlations for the energy-only and entropy-only test-set results. Thus, the results remain consistent with a conclusion that the energy term alone is enough to gain all the

benefit of the scoring functions. The only other major change, relative to the uncapped version of the scoring function, is that the fitted values of  $E_{\text{aff}}$  and  $S_{\text{aff}}$  changed from about  $-1.5 \text{ kcal/mol}$  to about  $-2.3 \text{ kcal/mol}$ , except that  $S_{\text{aff}}$  for the combined energy/entropy scoring function remained small. These increases presumably have the effect of compensating for the reduced values of the displacement function, i.e., for the fact that  $d_i^{\text{cap}} \leq d_i^{\text{nocap}}$  in eqs 2 and 3.

In order to further test the statistical significance of the HSA scoring results, we shuffled the energies and entropies among hydration sites and then refitted all six HSA-based scoring functions with the shuffled data. As summarized in the last six rows of Table 1, the uncapped scoring functions now yield poor correlations with experimental data ( $R^2 \approx 0.4$ ), just as observed for GIST, and the correlations for the capped scoring functions fall even lower. These results support the significance of the correlations obtained with the actual (unshuffled) data. The fact that the shuffled results are worse for the capped HSA scoring functions suggests, but does not prove, that applying the physically reasonable cap might reduce spurious correlations.

It is of interest to examine the locations of HSA scoring sites relative to the GIST scoring regions. We focus here on the energy-only scoring functions, since it is not clear that including entropy adds useful information, at least for FXa within the present functional form. As shown in Figure 4 (left), the HSA sites do not capture the complex shapes of the GIST scoring regions, and substantial parts of the GIST scoring region are entirely missed by the HSA scoring sites. These regions could presumably be used to direct rational lead drug design. The spatial relationship of the scoring sites to the ligands studied here may be appreciated from Figure 4 (right), which shows the van der Waals surface of a representative ligand.

#### 4. DISCUSSION

A key result of this first application of GIST to protein–ligand modeling is that the detailed representation of water structure and thermodynamics it affords works at least as well in a simple scoring function as the prior<sup>12</sup> and present site-based HSA implementations. In addition, the GIST results converge well within 5–10 ns of MD simulation time, depending upon whether one uses the energy-only model or the energy/entropy model. These simulation times are commensurate with those normally used for the HSA approach; see the Methods. Thus, the two approaches provide similar overall performance in the present application. Additional considerations include the fact that site-based approaches may require less data storage and that they paint a simple picture of water structure in a protein binding site. On the other hand, the GIST grid files produced are still small (<1 MB), and we anticipate that the more detailed rendering of hydration structure and thermodynamics afforded by the grid approach will be useful for insight and prediction. Note, in particular, that there are HSA sites which are only partly occupied by the more refined GIST scoring regions, as well as GIST scoring regions that are not identified by the HSA model, as evident from Figure 4. More generally, the fact that GIST is a more direct representation of the common underlying inhomogeneous solvation theory facilitates the interpretation of its results and provides clear pathways to future enhancements, such as the incorporation of higher-order correlations, as touched on below. A fast implementation of GIST, based upon focused grand canonical Monte Carlo

sampling,<sup>59</sup> may be of particular interest in the near term for high-throughput applications.

Another novel and striking result of the present study is that both the GIST and HSA models provide clear signals that ligands can gain affinity by displacing energetically unfavorable binding site water, whereas the displacement of entropically unfavorable water seems to play a negligible role. The energetically unfavorable water highlighted by this study localizes at hydrophobic patches of the protein surface, perhaps especially in concave regions where water molecules are expected to lose hydrogen bonds.<sup>60</sup> The concept that energy may outweigh entropy in cases of strong hydrophobic binding has been raised before,<sup>61,62</sup> in both experimental<sup>8,63–66</sup> and computational<sup>67,68</sup> contexts. Nonetheless, water entropy is typically thought to play a central role in hydrophobic binding.<sup>69–72</sup> Here, interestingly, neither the GIST or HSA models made a compelling case that the displacement of entropically unfavorable water consistently enhances affinity. We conjecture that the lack of a clear correlation of water entropy with affinity may reflect the fact that low water entropy often results from energetically favorable water–protein interactions, so that water may actually be quite stable in many locations where its entropy is low. This view is consistent with the experimental observation that the entropy of hydration of small ions is strongly negative,<sup>73</sup> although the free energy is also strongly negative. It may be possible in the future to devise a more sophisticated scoring function that would account for the enthalpy–entropy compensation between stabilizing energy and destabilizing entropy and focus on regions where this compensation breaks down, such as in the binding cavity of the synthetic host molecule cucurbit[7]uril.<sup>28</sup> It is also worth mentioning that different protein binding sites affect water differently, so a different result might be obtained for a different protein. Finally, it may be that capturing the entropic aspect of the hydrophobic effect requires accounting for water–water correlations, which are absent from the one-body entropy considered here. If so, the entropy term may become more important once pairwise correlations have been incorporated into GIST’s entropy calculations.

Our observation that the displacement of high energy water plays a greater role in ligand scoring than displacement of low entropy water appears to contrast with a prior HSA-based study of the same system, where the fitted scoring function placed approximately equal weight on water energy and entropy.<sup>12</sup> However, the range of fitted values for  $S_{\text{aff}}$  in our HSA models nearly spans the value of  $0.66 \text{ kcal/mol}$  for the corresponding parameter in the prior study,  $S_{\text{rwd}}$ . In addition, the prior study did not examine the uncertainty in its fitted energy and entropy parameters or evaluate a scoring function based purely on water energy. Therefore, the results of these two studies should not be regarded as inconsistent.

In summary, the grid-based GIST method of extracting information about hydration thermodynamics from MD simulations with explicit water has provided encouraging results in its first application to protein–ligand binding. It thus appears to hold significant promise as a broadly applicable method of understanding the role of binding site water in protein–ligand binding, and as a tool to improve the accuracy of methods for discovering high affinity targeted ligands. It is anticipated that the detailed representation of water distributions and thermodynamics which GIST affords will make it particularly informative. We are currently working to develop such applications and to release an open-source implementation of

GIST within the AmberTools<sup>36</sup> software package for others to study and use.

## ■ ASSOCIATED CONTENT

### Supporting Information

Congeneric ligand pairs. This material is available free of charge via the Internet at <http://pubs.acs.org>

## ■ AUTHOR INFORMATION

### Corresponding Authors

\*E-mail: mgilson@ucsd.edu.

\*E-mail: thomas.kurtzman@lehman.cuny.edu.

### Notes

The authors declare no competing financial interest.

## ■ ACKNOWLEDGMENTS

This publication was made possible in part by grants GM061300, GM100946, and GM095417 from the National Institutes of Health. Its contents are solely the responsibility of the authors and do not necessarily represent the official views of the NIH. We thank Dr. Hari Muddana for his assistance in generating RESP charges for the ligands.

## ■ REFERENCES

- (1) Ladbury, J. Just Add Water! The Effect of Water on the Specificity of Protein-Ligand Binding Sites and Its Potential Application to Drug Design. *Chem. Biol.* **1996**, *3*, 973–980.
- (2) Li, Z.; Lazaridis, T. Thermodynamic Contributions of the Ordered Water Molecule in HIV-1 Protease. *J. Am. Chem. Soc.* **2003**, *125*, 6636–6637.
- (3) García-Sosa, A. T.; Firth-Clark, S.; Mancera, R. L. Including Tightly-Bound Water Molecules in de Novo Drug Design. Exemplification through the in Silico Generation of Poly(ADP-Ribose)polymerase Ligands. *J. Chem. Inf. Model.* **2005**, *45*, 624–633.
- (4) Li, Z.; Lazaridis, T. Thermodynamics of Buried Water Clusters at a Protein-Ligand Binding Interface. *J. Phys. Chem. B* **2006**, *110*, 1464–1475.
- (5) Mancera, R. Molecular Modeling of Hydration in Drug Design. *Curr. Opin. Drug Discovery Dev.* **2007**, *10*, 275–280.
- (6) Wong, S.; Lightstone, F. Accounting for Water Molecules in Drug Design. *Expert Opin. Drug Discovery* **2011**, *6*, 65–74.
- (7) Poornima, C. S.; Dean, P. M. Hydration in Drug Design. 1. Multiple Hydrogen-Bonding Features of Water Molecules in Mediating Protein-Ligand Interactions. *J. Comput.-Aided Mol. Des.* **1995**, *9*, 500–512.
- (8) Young, T.; Abel, R.; Kim, B.; Berne, B. J.; Friesner, R. A. Motifs for Molecular Recognition Exploiting Hydrophobic Enclosure in Protein-Ligand Binding. *Proc. Natl. Acad. Sci. U. S. A.* **2007**, *104*, 808–813.
- (9) Bissantz, C.; Kuhn, B.; Stahl, M. A Medicinal Chemist's Guide to Molecular Interactions. *J. Med. Chem.* **2010**, *53*, 5061–5084.
- (10) Baron, R.; Setny, P.; Andrew McCammon, J. Water in Cavity–Ligand Recognition. *J. Am. Chem. Soc.* **2010**, *132*, 12091–12097.
- (11) Riniker, S.; Barandun, L. J.; Diederich, F.; Krämer, O.; Steffen, A.; van Gunsteren, W. F. Free Enthalpies of Replacing Water Molecules in Protein Binding Pockets. *J. Comput.-Aided Mol. Des.* **2012**, *26*, 1293–1309.
- (12) Abel, R.; Young, T.; Farid, R.; Berne, B. J.; Friesner, R. A. Role of the Active-Site Solvent in the Thermodynamics of Factor Xa Ligand Binding. *J. Am. Chem. Soc.* **2008**, *130*, 2817–2831.
- (13) Abel, R.; Wang, L.; Friesner, R. A.; Berne, B. J. A Displaced-Solvent Functional Analysis of Model Hydrophobic Enclosures. *J. Chem. Theory Comput.* **2010**, *6*, 2924–2934.
- (14) Hummer, G. Molecular Binding: Under Water's Influence. *Nat. Chem.* **2010**, *2*, 906–907.
- (15) Green, H. S. *The Molecular Theory of Fluids*; North-Holland Publishing Company: Amsterdam, 1952.
- (16) Nettleton, R. E.; Green, M. S. Expression in Terms of Molecular Distribution Functions for the Entropy Density in an Infinite System. *J. Chem. Phys.* **1958**, *29*, 1365.
- (17) Wallace, D. C. On the Role of Density Fluctuations in the Entropy of a Fluid. *J. Chem. Phys.* **1987**, *87*, 2282.
- (18) Baranyai, A.; Evans, D. J. Direct Entropy Calculation from Computer Simulation of Liquids. *Phys. Rev. A* **1989**, *40*, 3817.
- (19) Morita, T.; Hiroike, K. A New Approach to the Theory of Classical Fluids. III. *Prog. Theor. Phys.* **1961**, *25*, 537–578.
- (20) Lazaridis, T. Inhomogeneous Fluid Approach to Solvation Thermodynamics. 1. Theory. *J. Phys. Chem. B* **1998**, *102*, 3531–3541.
- (21) Lazaridis, T. Inhomogeneous Fluid Approach to Solvation Thermodynamics. 2. Applications to Simple Fluids. *J. Phys. Chem. B* **1998**, *102*, 3542–3550.
- (22) Kovalenko, A.; Hirata, F. Three-Dimensional Density Profiles of Water in Contact with a Solute of Arbitrary Shape: A RISM Approach. *Chem. Phys. Lett.* **1998**, *290*, 237–244.
- (23) Imai, T.; Kovalenko, A.; Hirata, F. Solvation Thermodynamics of Protein Studied by the 3D-RISM Theory. *Chem. Phys. Lett.* **2004**, *395*, 1–6.
- (24) Genheden, S.; Luchko, T.; Gusarov, S.; Kovalenko, A.; Ryde, U. An MM/3D-RISM Approach for Ligand Binding Affinities. *J. Phys. Chem. B* **2010**, *114*, 8505–8516.
- (25) Li, Z.; Lazaridis, T. Computing the Thermodynamic Contributions of Interfacial Water. *Methods Mol. Biol.* **2012**, *819*, 393–404.
- (26) Czapiewski, D.; Zielkiewicz, J. Structural Properties of Hydration Shell Around Various Conformations of Simple Poly-peptides. *J. Phys. Chem. B* **2010**, *114*, 4536–4550.
- (27) Haider, K.; Huggins, D. J. Combining Solvent Thermodynamic Profiles with Functionality Maps of the Hsp90 Binding Site to Predict the Displacement of Water Molecules. *J. Chem. Inf. Model.* **2013**, *53*, 2571–2586.
- (28) Nguyen, C. N.; Kurtzman Young, T.; Gilson, M. K. Grid Inhomogeneous Solvation Theory: Hydration Structure and Thermodynamics of the Miniature Receptor cucurbit[7]uril. *J. Chem. Phys.* **2012**, *137*, 044101.
- (29) Nguyen, C.; Gilson, M. K.; Young, T. Structure and Thermodynamics of Molecular Hydration via Grid Inhomogeneous Solvation Theory. 2011. arXiv: 1108.4876.
- (30) Singh, H.; Misra, S.; Hnizdo, V.; Fedorowicz, A.; Demchuk, E. Nearest Neighbor Estimates of Entropy. *Am. J. Math. Manage. Sci.* **2003**, *23*, 301–321.
- (31) Hnizdo, V.; Darian, E.; Fedorowicz, A.; Demchuk, E.; Li, S.; Singh, H. Nearest-Neighbor Nonparametric Method for Estimating the Configurational Entropy of Complex Molecules. *J. Comput. Chem.* **2007**, *28*, 655–668.
- (32) Bondi, A. Van Der Waals Volumes and Radii. *J. Phys. Chem.* **1964**, *68*, 441–451.
- (33) Pearlstein, R. A.; Hu, Q.-Y.; Zhou, J.; Yowe, D.; Levell, J.; Dale, B.; Kaushik, V. K.; Daniels, D.; Hanrahan, S.; Sherman, W.; Abel, R. New Hypotheses about the Structure–function of Proprotein Convertase Subtilisin/kexin Type 9: Analysis of the Epidermal Growth Factor-like Repeat A Docking Site Using WaterMap. *Proteins: Struct., Funct., Bioinf.* **2010**, *78*, 2571–2586.
- (34) Abel, R.; Salam, N. K.; Shelley, J.; Farid, R.; Friesner, R. A.; Sherman, W. Contribution of Explicit Solvent Effects to the Binding Affinity of Small-Molecule Inhibitors in Blood Coagulation Factor Serine Proteases. *ChemMedChem* **2011**, *6*, 1049–1066.
- (35) Beuming, T.; Che, Y.; Abel, R.; Kim, B.; Shanmugasundaram, V.; Sherman, W. Thermodynamic Analysis of Water Molecules at the Surface of Proteins and Applications to Binding Site Prediction and Characterization. *Proteins: Struct., Funct., Bioinf.* **2012**, *80*, 871–883.
- (36) Case, D. A.; Darden, T. A.; Cheatham, T. E., III; Simmerling, C. L.; Wang, J.; Duke, R. E.; Luo, R.; Walker, R. C.; Zhang, W.; Merz, K. M.; Roberts, B. P.; Hayik, S.; Roitberg, A. E.; Seabra, G.; Swails, J. M.; Kolossváry, I.; Wong, K. F.; Paesani, F.; Vanicek, J.; Wolf, R. M.; Liu,

- J.; Wu, X.; Brozell, S. R.; Steinbrecher, T.; Gohlke, H.; Cai, Q.; Ye, X.; Wang, J.; Hsieh, M.-J.; Cui, G.; Roe, D. R.; Mathews, D. H.; Seetin, M. G.; Salomon-Ferrer, R.; Sagui, C.; Babin, V.; Luchko, T.; Gusarov, S.; Kovalenko, A.; Kollman, P. A. AMBER 12; University of California: San Francisco, 2012.
- (37) Bernstein, F. C.; Koetzle, T. F.; Williams, T. F.; G. J. B. Meyer, J.; Brice, M. D.; Rodgers, J. R.; Kennard, O.; Shimanouchi, T.; Tasumi, M. The Protein Data Bank: A Computer-Based Archival File for Macromolecular Structures. *J. Mol. Biol.* **1977**, *112*, 535–542.
- (38) Berman, H. M.; Westbrook, J.; Feng, Z.; Gilliland, G.; Bhat, T. N.; Weissig, H.; Shindyalov, I. N.; Bourne, P. E. The Protein Data Bank. *Nucleic Acids Res.* **2000**, *28*, 235–242.
- (39) Adler, M.; Davey, D. D.; Phillips, G. B.; Kim, S. H.; Jancarik, J.; Rumennik, G.; Light, D. R.; Whitlow, M. Preparation, Characterization, and the Crystal Structure of the Inhibitor ZK-807834 (CI-1031) Complexed with Factor Xa. *Biochemistry* **2000**, *39*, 12534–12542.
- (40) Hornak, V.; Abel, R.; Okur, A.; Strockbine, B.; Roitberg, A.; Simmerling, C. Comparison of Multiple Amber Force Fields and Development of Improved Protein Backbone Parameters. *Proteins: Struct., Funct., Bioinf.* **2006**, *65*, 712–725.
- (41) Jorgensen, W. L.; Chandrasekhar, J.; Madura, J. D.; Impey, R. W.; Klein, M. L. Comparison of Simple Potential Functions for Simulating Liquid Water. *J. Chem. Phys.* **1983**, *79*, 926.
- (42) Salomon-Ferrer, R.; Götz, A. W.; Poole, D.; Le Grand, S.; Walker, R. C. Routine Microsecond Molecular Dynamics Simulations with AMBER on GPUs. 2. Explicit Solvent Particle Mesh Ewald. *J. Chem. Theory Comput.* **2013**, *9*, 3878–3888.
- (43) Ryckaert, J.-P.; Ciccotti, G.; Berendsen, H. J. C. Numerical Integration of the Cartesian Equations of Motion of a System with Constraints: Molecular Dynamics of N-Alkanes. *J. Comput. Phys.* **1977**, *23*, 327–341.
- (44) Maignan, S.; Guilloteau, J. P.; Pouzieux, S.; Choi-Sledeski, Y. M.; Becker, M. R.; Klein, S. I.; Ewing, W. R.; Pauls, H. W.; Spada, A. P.; Mikol, V. Crystal Structures of Human Factor Xa Complexed with Potent Inhibitors. *J. Med. Chem.* **2000**, *43*, 3226–3232.
- (45) Nar, H.; Bauer, M.; Schmid, A.; Stassen, J. M.; Wienen, W.; Pripke, H. W.; Kauffmann, I. K.; Ries, U. J.; Hauel, N. H. Structural Basis for Inhibition Promiscuity of Dual Specific Thrombin and Factor Xa Blood Coagulation Inhibitors. *Structure* **2001**, *9*, 29–37.
- (46) Adler, M.; Kochanny, M. J.; Ye, B.; Rumennik, G.; Light, D. R.; Biancalana, S.; Whitlow, M. Crystal Structures of Two Potent Nonamidine Inhibitors Bound to Factor Xa. *Biochemistry* **2002**, *41*, 15514–15523.
- (47) Guertin, K. R.; Gardner, C. J.; Klein, S. I.; Zulli, A. L.; Czekaj, M.; Gong, Y.; Spada, A. P.; Cheney, D. L.; Maignan, S.; Guilloteau, J.-P.; Brown, K. D.; Colussi, D. J.; Chu, V.; Heran, C. L.; Morgan, S. R.; Bentley, R. G.; Dunwiddie, C. T.; Leadley, R. J.; Pauls, H. W. Optimization of the Beta-Aminoester Class of Factor Xa Inhibitors. Part 2: Identification of FXV673 as a Potent and Selective Inhibitor with Excellent In Vivo Anticoagulant Activity. *Bioorg. Med. Chem. Lett.* **2002**, *12*, 1671–1674.
- (48) Maignan, S.; Guilloteau, J.-P.; Choi-Sledeski, Y. M.; Becker, M. R.; Ewing, W. R.; Pauls, H. W.; Spada, A. P.; Mikol, V. Molecular Structures of Human Factor Xa Complexed with Ketopiperazine Inhibitors: Preference for a Neutral Group in the S1 Pocket. *J. Med. Chem.* **2003**, *46*, 685–690.
- (49) Matter, H.; Will, D. W.; Nazaré, M.; Schreuder, H.; Laux, V.; Wehner, V. Structural Requirements for Factor Xa Inhibition by 3-Oxybenzamides with Neutral P1 Substituents: Combining X-Ray Crystallography, 3D-QSAR, and Tailored Scoring Functions. *J. Med. Chem.* **2005**, *48*, 3290–3312.
- (50) Haginoya, N.; Kobayashi, S.; Komoriya, S.; Yoshino, T.; Suzuki, M.; Shimada, T.; Watanabe, K.; Hirokawa, Y.; Furugori, T.; Nagahara, T. Synthesis and Conformational Analysis of a Non-Amidine Factor Xa Inhibitor That Incorporates 5-Methyl-4,5,6,7-tetrahydrothiazolo-[5,4-C]pyridine as S4 Binding Element. *J. Med. Chem.* **2004**, *47*, 5167–5182.
- (51) Young, R. J.; Campbell, M.; Borthwick, A. D.; Brown, D.; Burns-Kurtis, C. L.; Chan, C.; Convery, M. A.; Crowe, M. C.; Dayal, S.; Diallo, H.; Kelly, H. A.; King, N. P.; Kleanthous, S.; Mason, A. M.; Mordaunt, J. E.; Patel, C.; Pateman, A. J.; Senger, S.; Shah, G. P.; Smith, P. W.; Watson, N. S.; Weston, H. E.; Zhou, P. Structure- and Property-Based Design of Factor Xa Inhibitors: Pyrrolidin-2-Ones with Acyclic Alanyl Amides as P4Motifs. *Bioorg. Med. Chem. Lett.* **2006**, *16*, 5953–5957.
- (52) Quan, M. L.; Lam, P. Y. S.; Han, Q.; Pinto, D. J. P.; He, M. Y.; Li, R.; Ellis, C. D.; Clark, C. G.; Teleha, C. A.; Sun, J.-H.; Alexander, R. S.; Bai, S.; Luetgen, J. M.; Knabb, R. M.; Wong, P. C.; Wexler, R. R. Discovery of 1-(3'-Aminobenzisoxazol-5'-Yl)-3-Trifluoromethyl-N-[2-Fluoro-4-[(2'-Dimethylaminomethyl)imidazol-1-Yl]phenyl]-1H-Pyrazole-5-Carboxamide Hydrochloride (razaxaban), a Highly Potent, Selective, and Orally Bioavailable Factor Xa Inhibitor. *J. Med. Chem.* **2005**, *48*, 1729–1744.
- (53) Nazaré, M.; Will, D. W.; Matter, H.; Schreuder, H.; Ritter, K.; Urmann, M.; Essrich, M.; Bauer, A.; Wagner, M.; Czech, J.; Lorenz, M.; Laux, V.; Wehner, V. Probing the Subpockets of Factor Xa Reveals Two Binding Modes for Inhibitors Based on a 2-Carboxyindole Scaffold: A Study Combining Structure-Activity Relationship and X-Ray Crystallography. *J. Med. Chem.* **2005**, *48*, 4511–4525.
- (54) Pinto, D. J. P.; Orwat, M. J.; Quan, M. L.; Han, Q.; Galemmo, R. A., Jr.; Amparo, E.; Wells, B.; Ellis, C.; He, M. Y.; Alexander, R. S.; Rossi, K. A.; Smallwood, A.; Wong, P. C.; Luetgen, J. M.; Rendina, A. R.; Knabb, R. M.; Mersinger, L.; Kettner, C.; Bai, S.; He, K.; Wexler, R. R.; Lam, P. Y. S. 1-[3-Aminobenzisoxazol-5'-Yl]-3-Trifluoromethyl-6-[2'-(3-(R)-Hydroxy-N-Pyrrolidinyl)methyl-[1,1']-Biphen-4-Yl]-1,4,5,6-Tetrahydropyrazolo-[3,4-C]-Pyridin-7-One (BMS-740808) a Highly Potent, Selective, Efficacious, and Orally Bioavailable Inhibitor of Blood Coagulation Factor Xa. *Bioorg. Med. Chem. Lett.* **2006**, *16*, 4141–4147.
- (55) Matter, H.; Defossa, E.; Heinelt, U.; Blohm, P.-M.; Schneider, D.; Müller, A.; Herok, S.; Schreuder, H.; Liesum, A.; Brachvogel, V.; Lönze, P.; Walser, A.; Al-Obeidi, F.; Wildgoose, P. Design and Quantitative Structure-Activity Relationship of 3-Amidinobenzyl-1H-Indole-2-Carboxamides as Potent, Nonchiral, and Selective Inhibitors of Blood Coagulation Factor Xa. *J. Med. Chem.* **2002**, *45*, 2749–2769.
- (56) Bayly, C. I.; Cieplak, P.; Cornell, W. D.; Kollman, P. A. A Well-Behaved Electrostatic Potential Based Method Using Charge-Restraints for Deriving Charges: The RESP Model. *J. Phys. Chem.* **1993**, *97*, 10269–10280.
- (57) Wang, J.; Wolf, R.; Caldwell, J.; Kollman, P.; Case, D. Development and Testing of a General Amber Force Field. *J. Comput. Chem.* **2004**, *25*, 1157–1174.
- (58) Humphrey, W.; Dalke, A.; Schulten, K. VMD -Visual Molecular Dynamics. *J. Mol. Graphics* **1996**, *14*, 33–38.
- (59) Raman, E. P.; MacKerrell, A. D., Jr. Rapid Estimation of Hydration Thermodynamics of Macromolecular Regions. *J. Chem. Phys.* **2013**, *139*, 055105.
- (60) Sharp, K.; Nicholls, A.; Fine, R.; Honig, B. Reconciling the Magnitude of the Microscopic and Macroscopic Hydrophobic Effects. *Science* **1991**, *252*, 106–109.
- (61) Lazaridis, T. Hydrophobic Effect. In *eLS*; John Wiley & Sons, Ltd: Chichester, U. K., 2001.
- (62) Lazaridis, T. Hydrophobic Effect. *eLS*; John Wiley & Sons, Ltd: Chichester, U. K., 2013; pp 1–9.
- (63) Bingham, R. J.; Findlay, J. B. C.; Hsieh, S.-Y.; Kalverda, A. P.; Kjellberg, A.; Perazzolo, C.; Phillips, S. E. V.; Seshadri, K.; Trinh, C. H.; Turnbull, W. B.; Bodenhausen, G.; Homans, S. W. Thermodynamics of Binding of 2-Methoxy-3-Isopropylpyrazine and 2-Methoxy-3-Isobutylpyrazine to the Major Urinary Protein. *J. Am. Chem. Soc.* **2004**, *126*, 1675–1681.
- (64) Englert, L.; Biela, A.; Zayed, M.; Heine, A.; Hangauer, D.; Klebe, G. Displacement of Disordered Water Molecules from Hydrophobic Pocket Creates Enthalpic Signature: Binding of Phosphonamide to the S1'-Pocket of Thermolysin. *Biochim. Biophys. Acta, Gen. Subj.* **2010**, *1800*, 1192–1202.

- (65) Biela, A.; Nasief, N. N.; Betz, M.; Heine, A.; Hangauer, D.; Klebe, G. Dissecting the Hydrophobic Effect on the Molecular Level: The Role of Water, Enthalpy, and Entropy in Ligand Binding to Thermolysin. *Angew. Chem., Int. Ed.* **2013**, *52*, 1822–1828.
- (66) Young, T.; Hua, L.; Huang, X.; Abel, R.; Friesner, R.; Berne, B. J. Dewetting Transitions in Protein Cavities. *Proteins: Struct., Funct., Bioinf.* **2010**, *78*, 1856–1869.
- (67) Lemieux, R. U. How Water Provides the Impetus for Molecular Recognition in Aqueous Solution. *Acc. Chem. Res.* **1996**, *29*, 373–380.
- (68) Setny, P.; Baron, R.; McCammon, J. A. How Can Hydrophobic Association Be Enthalpy Driven? *J. Chem. Theory Comput.* **2010**, *6*, 2866–2871.
- (69) Frank, H. S.; Evans, M. W. Free Volume and Entropy in Condensed Systems III. Entropy in Binary Liquid Mixtures; Partial Molal Entropy in Dilute Solutions; Structure and Thermodynamics in Aqueous Electrolytes. *J. Chem. Phys.* **1945**, *13*, 507.
- (70) Kauzmann, W. Some Factors in the Interpretation of Protein Denaturation. *Adv. Prot. Chem.* **1959**, *14*, 1–63.
- (71) Eisenberg, D.; Kauzmann, W. *The Structure and Properties of Water*; 1st ed.; Oxford University Press: New York, 1969.
- (72) Ashbaugh, H. S.; Paulaitis, M. E. Entropy of Hydrophobic Hydration: Extension to Hydrophobic Chains. *J. Phys. Chem.* **1996**, *100*, 1900–1913.
- (73) Marcus, Y.; Loewenschuss, A. Chapter 4. Standard Entropies of Hydration of Ions. *Annu. Rep. Prog. Chem., Sect. C: Phys. Chem.* **1984**, *81*, 81–135.